Supporting Information

Ultrafast Pressure Sensing with Transient Tunnelling Currents

Ashok S. Chauhan, Isaac Taylor-Harrod, Samuel D. Littlejohn, Alain Nogaret
Department of Physics, University of Bath, Bath BA2 7AY, UK

1. Experimental method for generating calibrated stress

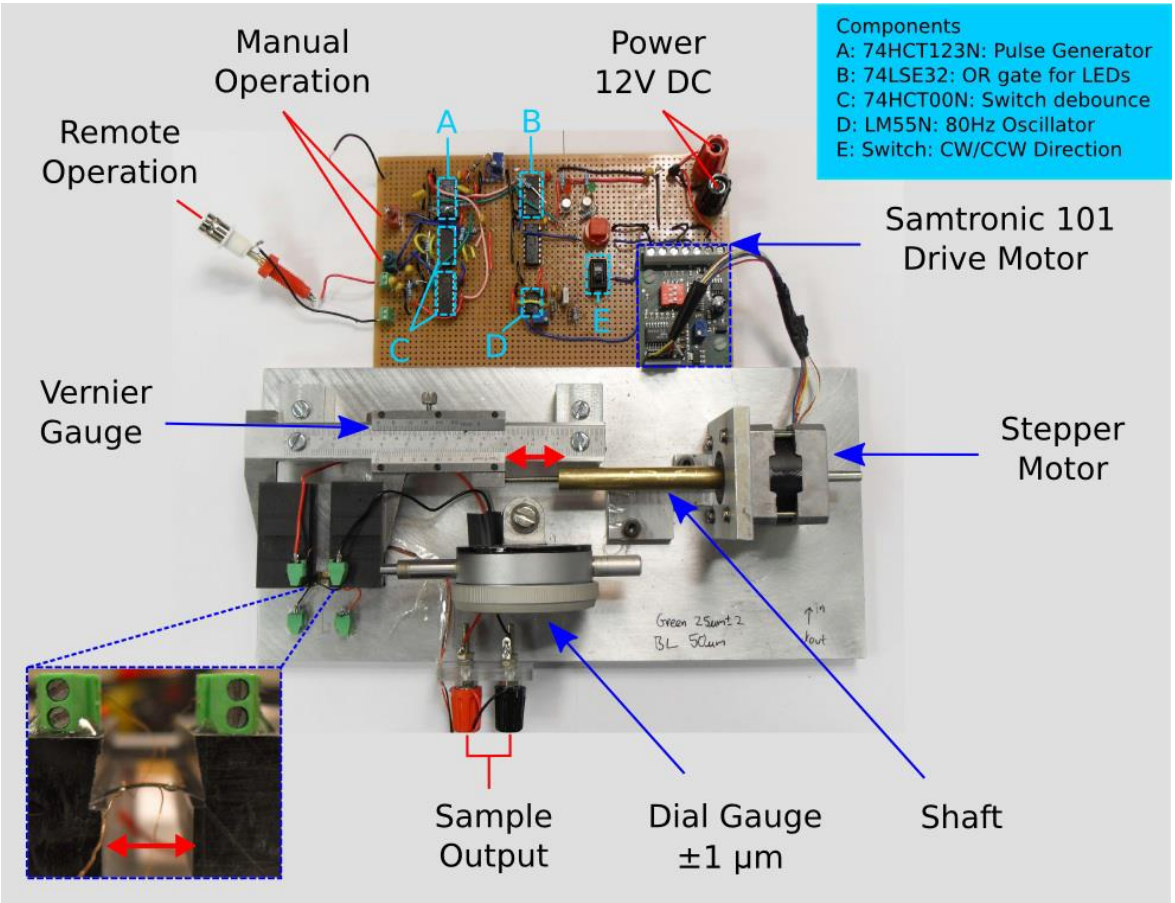

Figure S1 – Computer controlled rig used to stress the composite in Fig.1a, 1b and Fig.3a
A purpose built stepper motor bench applies precisely controlled bends to the bilayer. The bench functions as a linear actuator that slides the right clamp of the Vernier by small horizontal steps Δl=200µm which bend the bilayer (inset). The lead screw has a ¼ inch Whitworth thread with a pitch of 0.05 inch (20 threads per inch). Hence a screw rotation of 56° corresponds approximately to a 200µm horizontal displacement. This displacement was calibrated using the dial gauge (accuracy ±1µm). Motor action was triggered by a rising signal edge remotely applied by a Labview program. The program simultaneously records the 4 terminal resistance of the composite. *Inset*: detail of the PEN/composite bilayer bent by varying the distance between the clamps (red arrow).

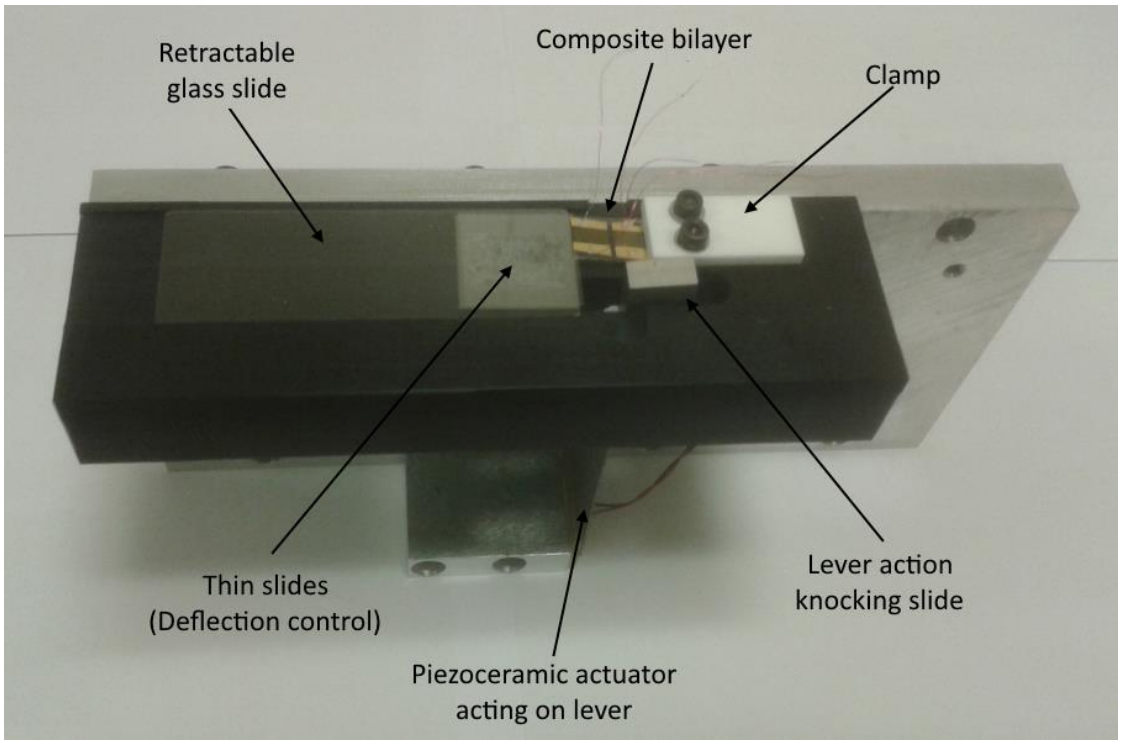

Figure S2 – Piezoceramic actuator used to resolve the piezoresistance rise time in Fig.3c.
The actuator applies a single stress step to the composite film (Piezo-systems, PSI-5A4E). It has a response time of 1µs which is sufficient to resolve the rise time of the piezoresistance (~ms). The composite bilayer was clamped at one end and bent upwards by raising the other end with a retractable glass slide. A voltage step applied to the piezoceramic actuator retracts the glass slide and releases the strain. The magnitude and repeatability of the stress step is controlled by the thickness of the glass slide (100µm). The piezoresistance was measured using the 4 terminal method at a sampling rate of 20kHz.

2. Calculation of stress in the bent composite film

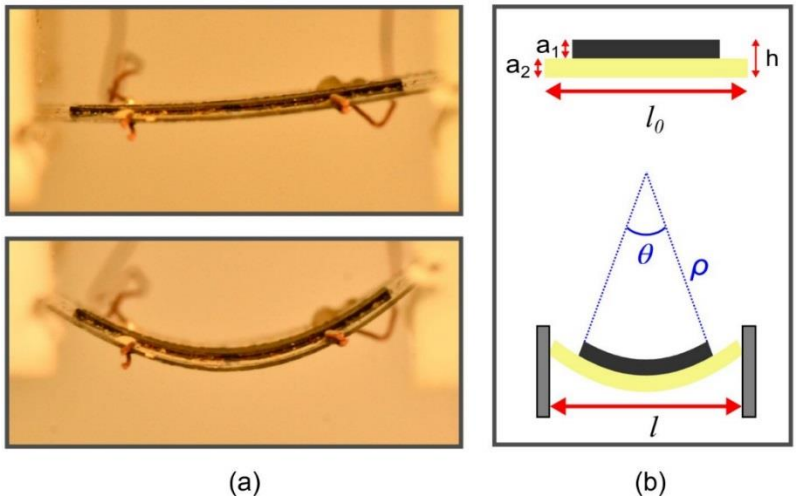

Figure S3 – (a) Composite-acetate bilayer. (b) Schematics of the experiment showing structural parameters of the bent bilayer: a_1, thickness of the **composite** film (layer 1) ; a_2, thickness of the **cellulose acetate** substrate (layer 2); l_0, substrate length; l, horizontal elongation; ρ, bend radius.

Layer	Young's modulus	Poisson ratio	Thickness
1. PDMS/HOPG composite[1]	E_1 : 1.8±0.05MPa	γ_1 : 0.4999±0.0001	a_1 : 100µm
2. Cellulose acetate[2] Sheet	E_2 : 41±11MPa	γ_2 : 0.391±0.008	a_2 : 100µm

Table S4 – Tabulated values of the model parameters[1,2]

In Fig.S3, the bend radius ρ relates to the compression ratio $\eta = (l_0 - l)/l_0$ through:

$$\left.\begin{aligned} l_0 &= \rho\theta \\ \frac{l}{2} &= \rho\sin\left(\frac{\theta}{2}\right) \end{aligned}\right\} \Rightarrow \; l = 2\rho\sin\left(\frac{l_0}{2\rho}\right),$$

$$l = l_0\frac{\sin\left(\frac{l_0}{2\rho}\right)}{\left(\frac{l_0}{2\rho}\right)} = l_0\,\mathrm{sinc}\left(\frac{l_0}{2\rho}\right),$$

Horizontal compression ratio

$$\eta = \frac{l_0 - l}{l_0} = 1 - \mathrm{sinc}\left(\frac{l_0}{2\rho}\right) \qquad \text{(S1)}$$

Taylor expansion: $x = \frac{l_0}{2\rho} \to 0$; $\eta = 1 - \frac{x - \frac{x^3}{3!}}{x} = \frac{x^2}{3!} \Rightarrow x = \sqrt{6\eta} \Rightarrow \frac{1}{\rho} = \frac{\sqrt{24\eta}}{l_0}$

Step *n*	0	1	2	3	4	5	6	7	8	9
$\Delta l = l - l_0$ µm	-200	-400	-600	-800	-1000	-1200	-1400	-1600	-1800	-2000
$\eta = (l - l_0)/l$ %	1.429	2.857	4.286	5.714	7.143	8.571	10.0	11.429	12.857	14.286
ρ mm	23.909	16.907	13.804	11.955	10.693	9.761	9.037	8.453	7.970	7.561
$\Delta_n(1/\rho)$ x10^{-6} µm^{-1}	30.331	17.324	13.293	11.207	9.8734	8.9262	8.2085	7.6403	7.1759	6.7871
$\Delta_n\varepsilon_{xx}$ %	-0.51	-0.29	-0.22	-0.19	-0.17	-0.15	-0.14	-0.13	-0.12	-0.11
$\Delta_n\varepsilon_{yy}$ %	+0.07	+0.04	+0.03	+0.03	+0.02	+0.02	+0.02	+0.02	+0.016	+0.015
$\Delta_n\varepsilon_{zz}$ %	+0.44	+0.25	+0.19	+0.16	+0.15	+0.13	+0.12	+0.11	+0.104	+0.095

Table S5 – 3D strain increment $\Delta\varepsilon_\alpha$ inferred from the compression ratio η using Eq.S1 and Eq.1

[1] RTV 137 data sheet Alchemie (E_{SiO}=1.3MPa), E_{HOPG}=12GPa and use the lower bound Young's modulus for mixtures:

[2] http://www.azom.com/properties.aspx?ArticleID=1461

3D stress increment $\Delta\sigma_{\alpha\alpha}$ induced by a change in substrate curvature radius: $\rho_{n-1} \rightarrow \rho_n$. The biaxial stress increases proportionally to $\Delta_n(1/\rho)=1/\rho_n-1/\rho_{n-1}$. It is given by Ohring[3] as:

Biaxial stress increment

$$\Delta_n\sigma^1_{xx} = \frac{E_2 a_2^3}{6(1-\gamma_2^2)a_1(a_1+a_2)}\Delta_n\left(\frac{1}{\rho}\right)$$
$$\Delta_n\sigma^1_{yy} = \frac{E_2 a_2^3 \gamma_2}{6(1-\gamma_2^2)a_1(a_1+a_2)}\Delta_n\left(\frac{1}{\rho}\right) \qquad \text{(S2)}$$
$$\Delta_n\sigma^1_{zz} = 0$$

Eq.S2 reduces to the well-known Stoney formula for bowl-like deformation and a thick substrate ($a_2 >> a_1$). Eq.S2 is an exact formula for the stress.

3. Verification of the linearity of the I-V curves at 77K

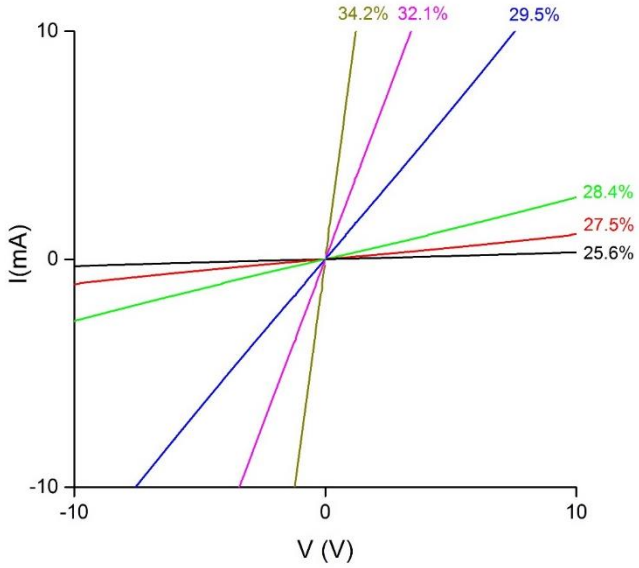

Figure S6 – Current-voltage characteristics at 77K

The I-V curves of composite devices at HOPG filling fractions between p=25.6% to p=34.2% are linear. The gold contact pads on the composite are Ohmic. Their resistance is 15 Ohms at p=25.6% and it decreases when the filling fraction increases.

[3] M. Ohring, The materials science of thin films, Academic Press, San Diego, 1992

4. Model predictions

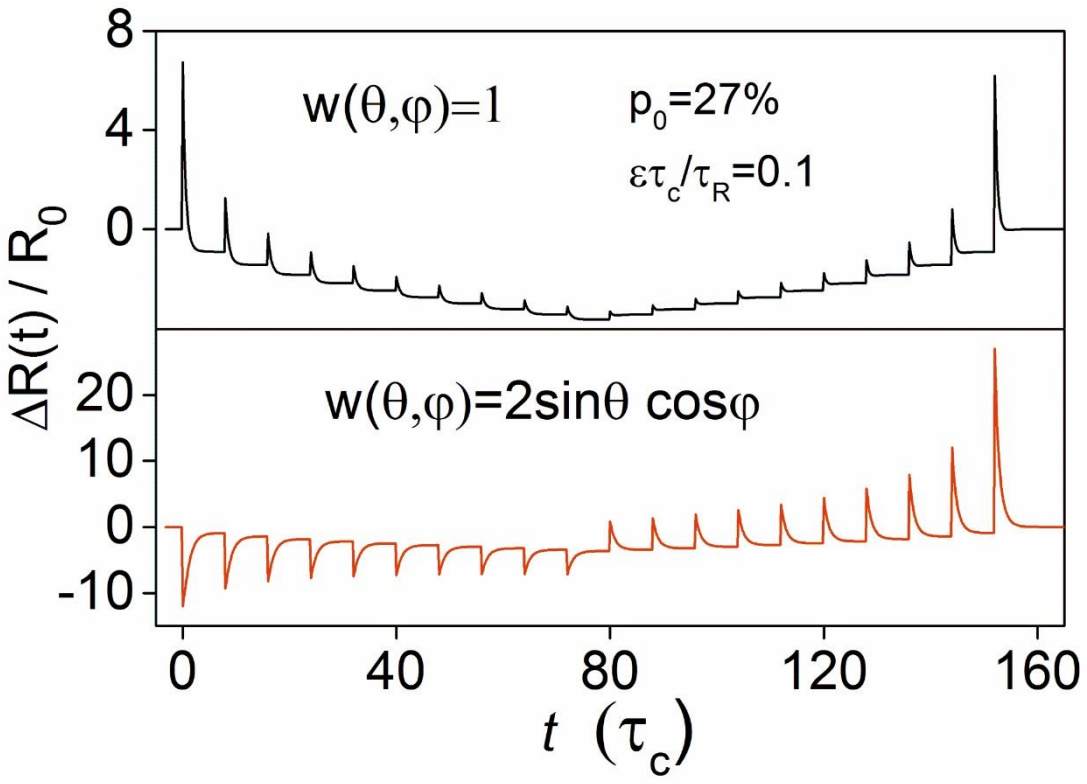

Figure S7 – Effects of the weight function calculated from Eq.2

The weight function $w(\theta,\varphi)$=1 (top) assumes that percolation follows a random walk through the composite whereas $w(\theta,\varphi)=2\sin\theta\cos\varphi$ (bottom) assumes percolation is driven by an electric field in the *x*-direction. The bottom panel shows that the latter assumption would imply the observation of *negative* resistance spikes during the compressive first half of the cycle: compression shortens the *x*-oriented bonds therefore the overall resistance decreases because of the greater weight given to these bonds. This behaviour is *never observed experimentally*. Instead, the experimental piezoresistance displays *symmetric positive spikes over a stress cycle*. Symmetric spikes are theoretically predicted when random walk hopping through an isotropic network is assumed. Stress as a perturbation therefore gives us important insight into the nature of microscopic hopping.

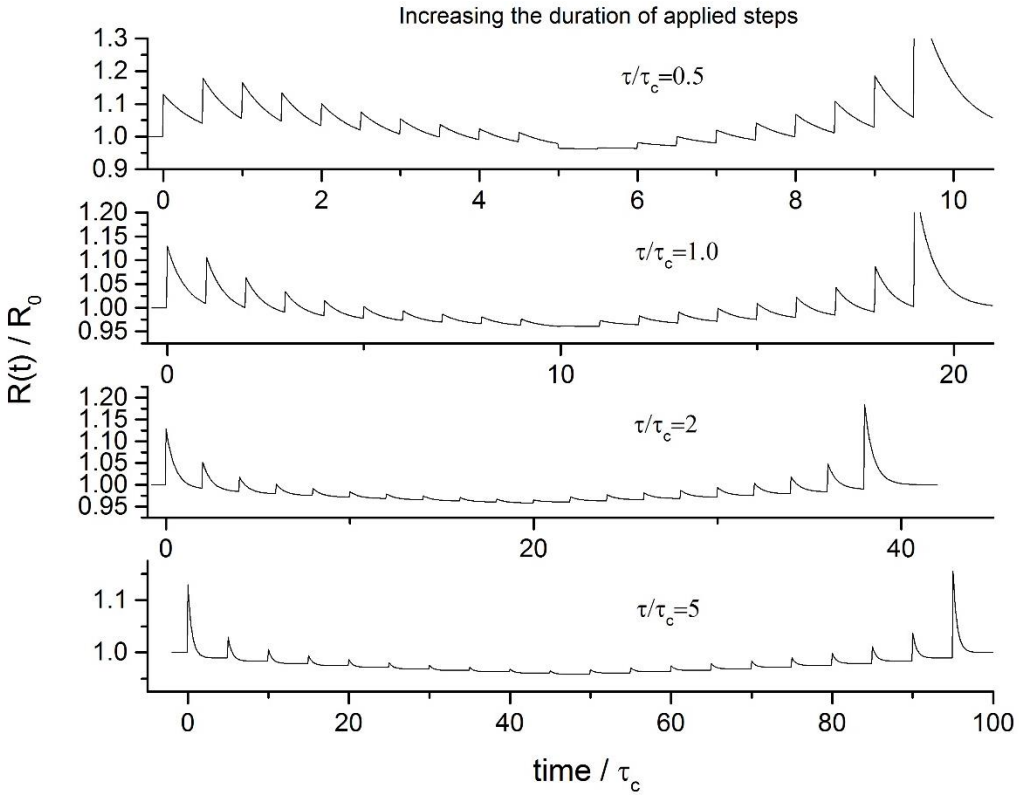

Figure S8 – Predicting the effect of increasing the duration of stress steps: M- to V- Shape
Theory predicts a transition from M-shaped to V-shaped piezoresistance as stress steps become longer in agreement with the experiment in Figs.1a,b. *Parameters:* $p_0 = 0.30$, $\varepsilon\tau_c/\tau_R = 0.2$; $\beta = 250\text{nm}^{-1}$.

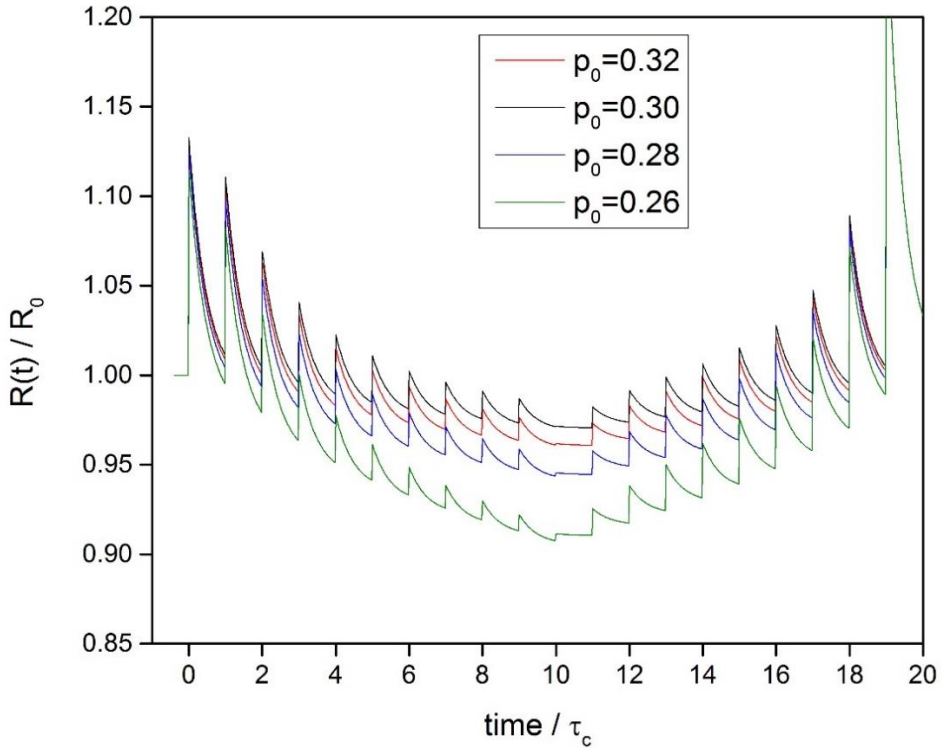

Figure S9 – Predicting the dependence of the resistance on HOPG filling fraction: p_0
The new equilibrium value of the resistance decreases with decreasing filling fraction as the tunnelling barrier becomes thicker. Thicker barriers produce a greater relative change in resistance.
Parameters: $\varepsilon\tau_c/\tau_R = 0.2$ (incomplete relaxation ratio), $\beta = 250\text{nm}^{-1}$ (inverse of tunnelling decay length).

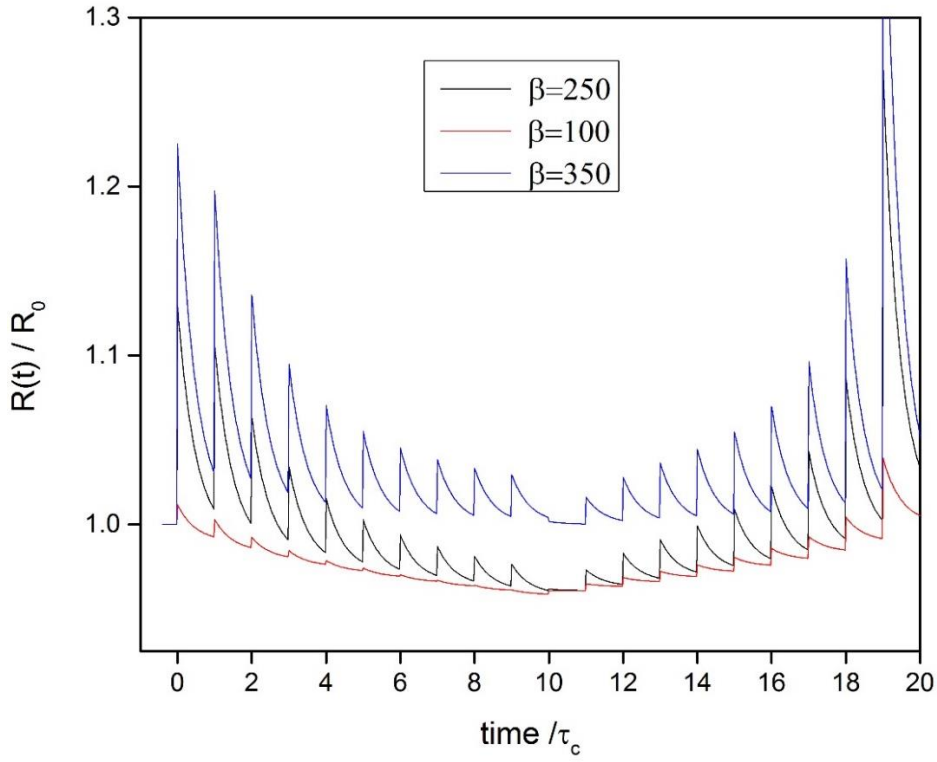

Figure S10 – Predicted effect of the tunnelling barrier height on the resistance spikes
The spike amplitude increases with the tunnelling barrier height V_0 ($\beta = 2\sqrt{2mV_0}/\hbar$). A comparable behaviour is observed when the width of the tunnelling barrier increases in Fig.3b.
Parameters: $\varepsilon\tau_c/\tau_R$ = 0.2, p_0 = 0.30.

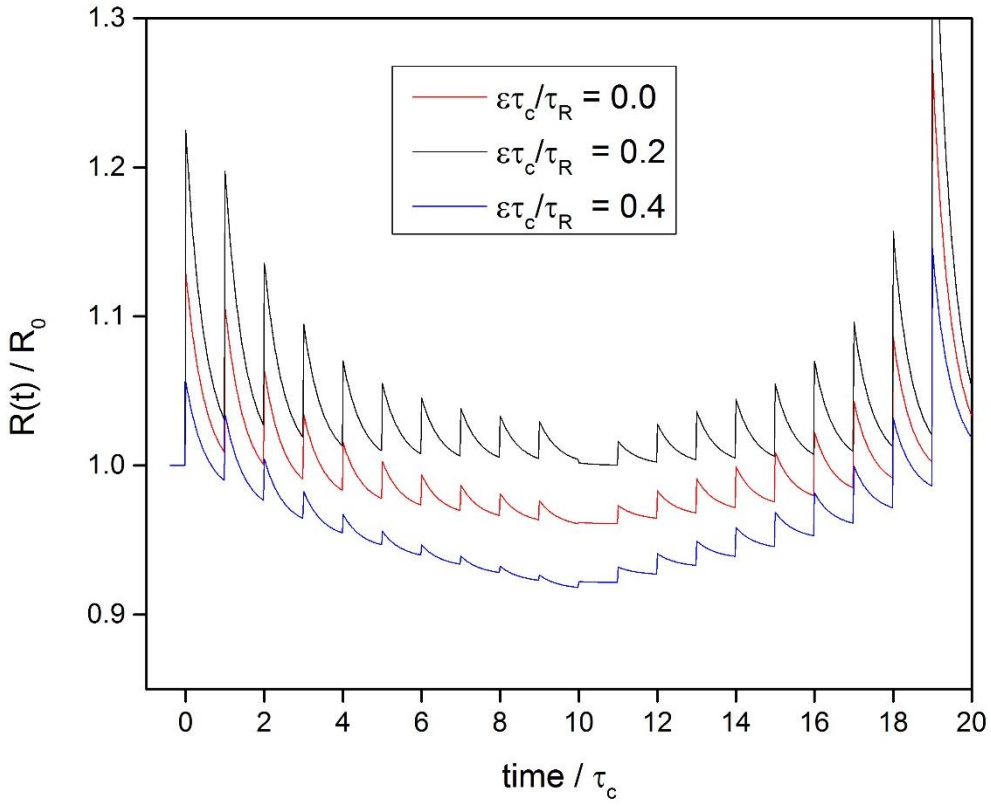

Figure S11 – Theoretical dependence of the resistance on the incomplete relaxation ratio: ε
Due to incomplete relaxation, the composite retains residual stress/deformation on a time scale larger than the viscoelastic relaxation times. Compressive stress decreases the mean hopping distance resulting in a drop in resistance.
Parameters: $p_0 = 0.30$, $\beta = 250\text{nm}^{-1}$.

5. Video of real time pressure imaging

This video shows real time pressure imaging with a 8x8 sensor array:
http://people.bath.ac.uk/pysarn/Pressure_imaging.m4v

6. Pressure sensor arrays

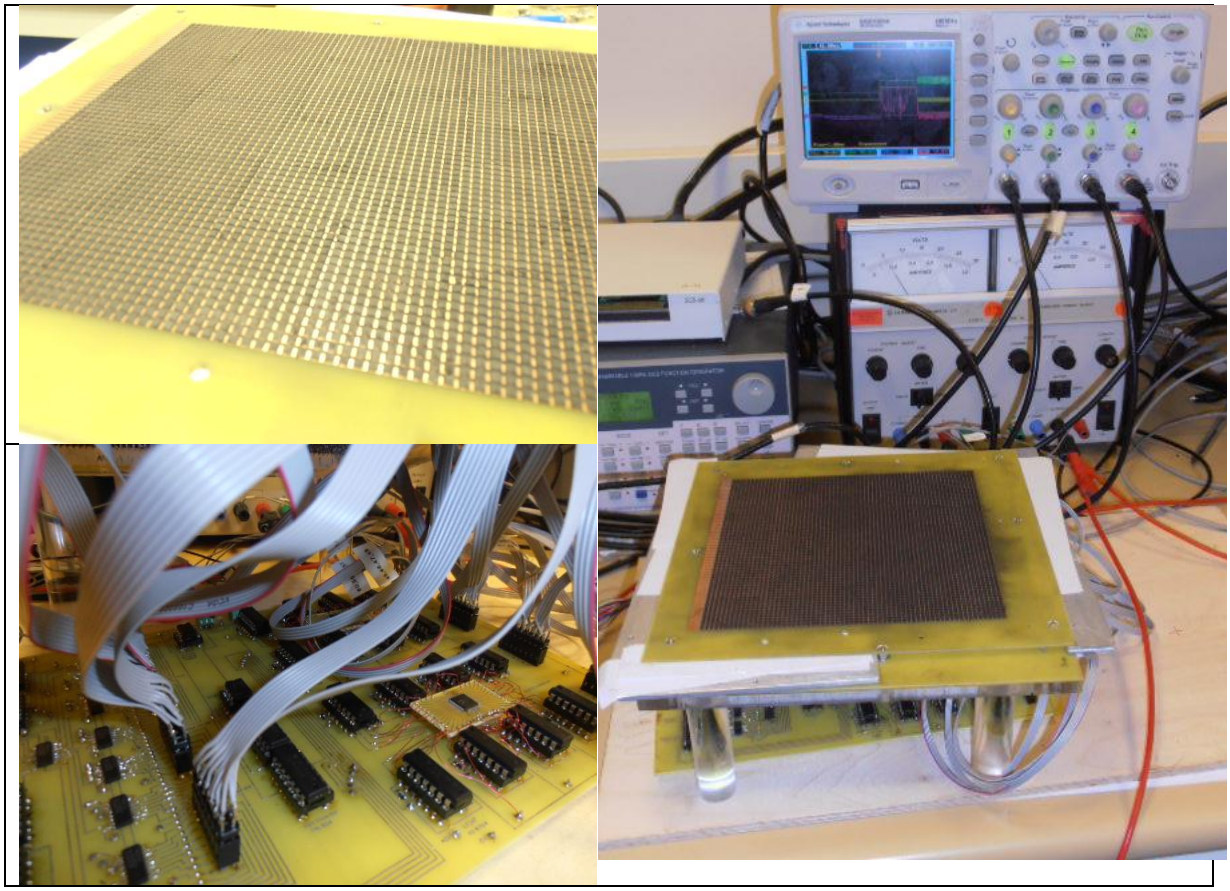

Figure S12 – Pressure sensor array
Top left: 64 x 64 array of composite elements with 0.1inch pitch. The copper electrodes at the left bias rows of 64 sensors at -5V. Composite elements stand atop ring electrodes which are kept at -5V. A gold plated pin passes through the centre of the ring to contact the composite. Applied pressure changes the resistance of the composite between pin and ring electrodes. The transient resistance $R(t)$ is read out by integrating the current i(t)=-5V/R(t) over a time interval of 5ms which is small compared to the viscoelactic relaxation time. All 64 sensing elements in the same row are addressed and read in parallel considerably increasing the imaging rate. **Bottom left:** Scan electronics of the array. **Right:** Pressure sensor array and scan electronics in operation.

7. SEM characterization of the composite and XRD of HOPG nanoparticles

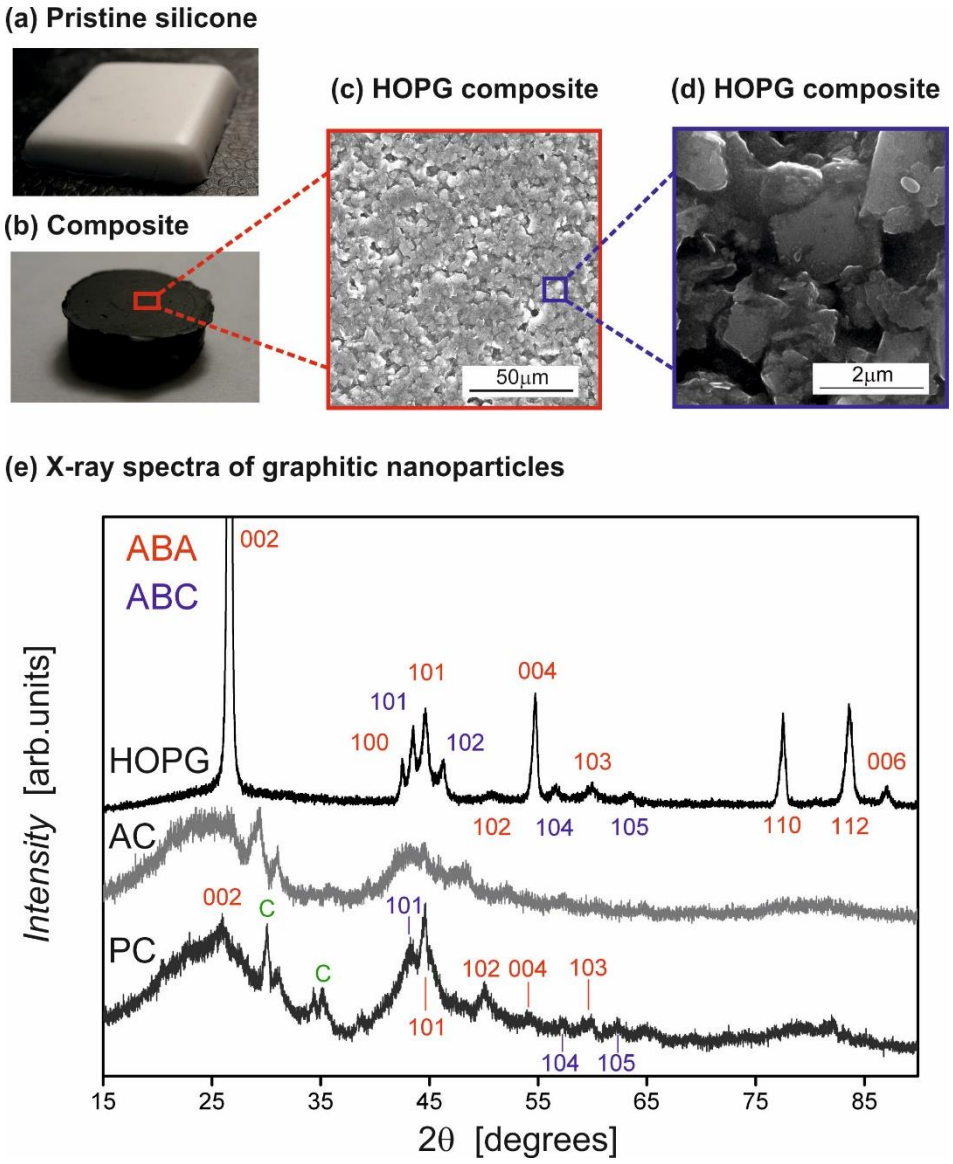

Figure S13 – **SEM micrographs of the composite and X-ray diffraction spectra of HOPG nanoparticles**

(a) Pristine PDMS rubber (Alchemie RTV 137).

(b) Conductive PDMS rubber obtained by mixing in **HOPG** nanoparticles.

(c) SEM micrograph of the **HOPG** composite showing an isotropic and homogeneous texture.

(d) Higher resolution SEM image of the **HOPG** composite showing the facets of individual nanoparticles i.e. the orientation of the graphite planes. The average particle size is 450nm. At the edges of nanoparticles the white lines represent the insulating silicone film that enhances the natural SEM contrast at the edges. The thickness of silicone separating nanoparticles is 50-100nm.

(e) XRD of graphite nanoparticles (**HOPG**), amorphous carbon nanoparticles (**AC**) and pyrolytic carbon nanoparticles (**PC**). The **HOPG** nanoparticles have graphene planes stacked in the two sequences ABA and ABC as evidenced by the (101) doublet. The **AC** nanoparticles are amorphous. The **PC** nanoparticles develop sp^2 covalent bonds as indicated by the resurgence of the (101) peaks. Their graphene layers however have random orientations as evidenced by the faint main diffraction peak. Covalent bonds between the graphene planes give rise to peaks **C**.

8. Image gallery of piezoresistive sensors

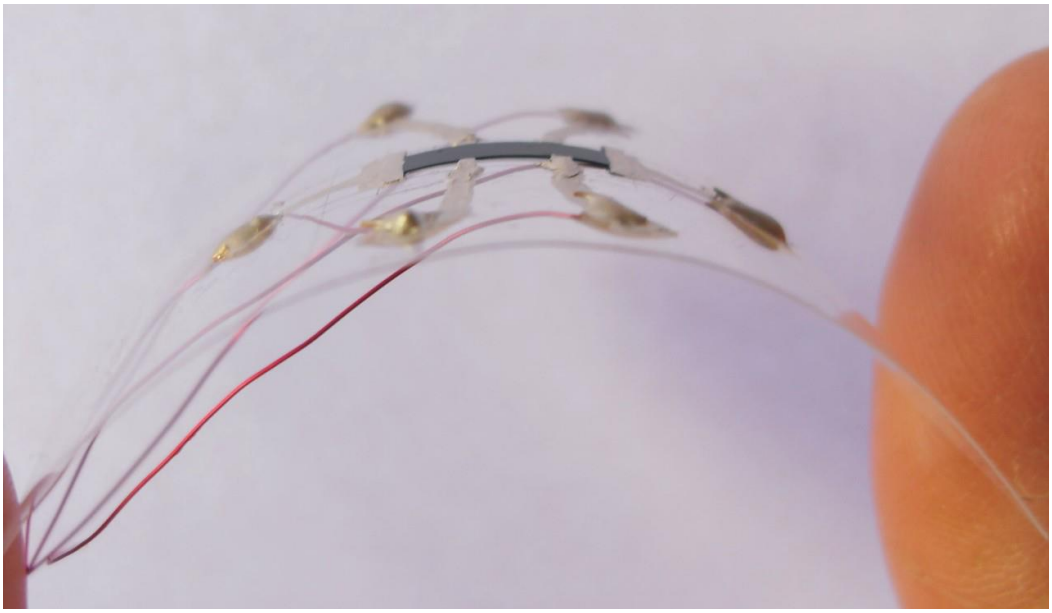

Figure S14 – **Sensor geometry for four terminal resistance measurements.**

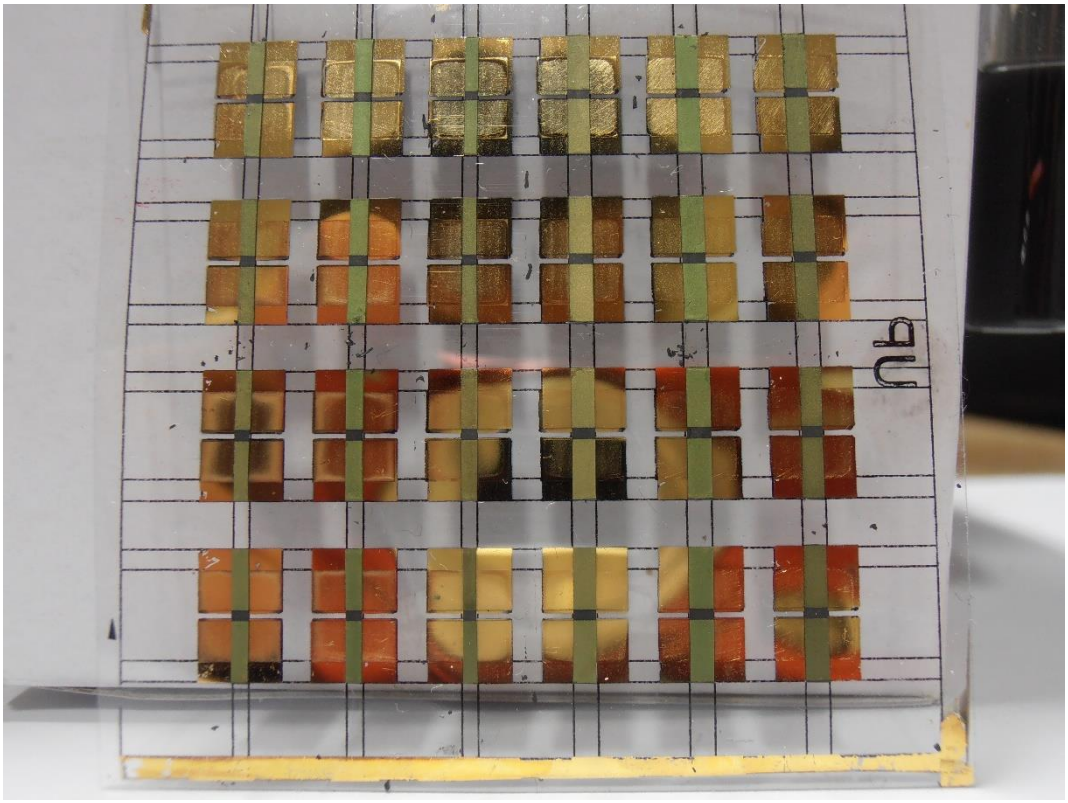

Figure S15 – **Sensor geometry for two-terminal resistance measurements**

Gold electrodes are deposited on the composite ribbon to obtain the low resistance Ohmic contacts needed to measure the two-terminal resistance. The width of the composite ribbon varies between 1mm and 3mm. The thickness of the composite film is 100μm.

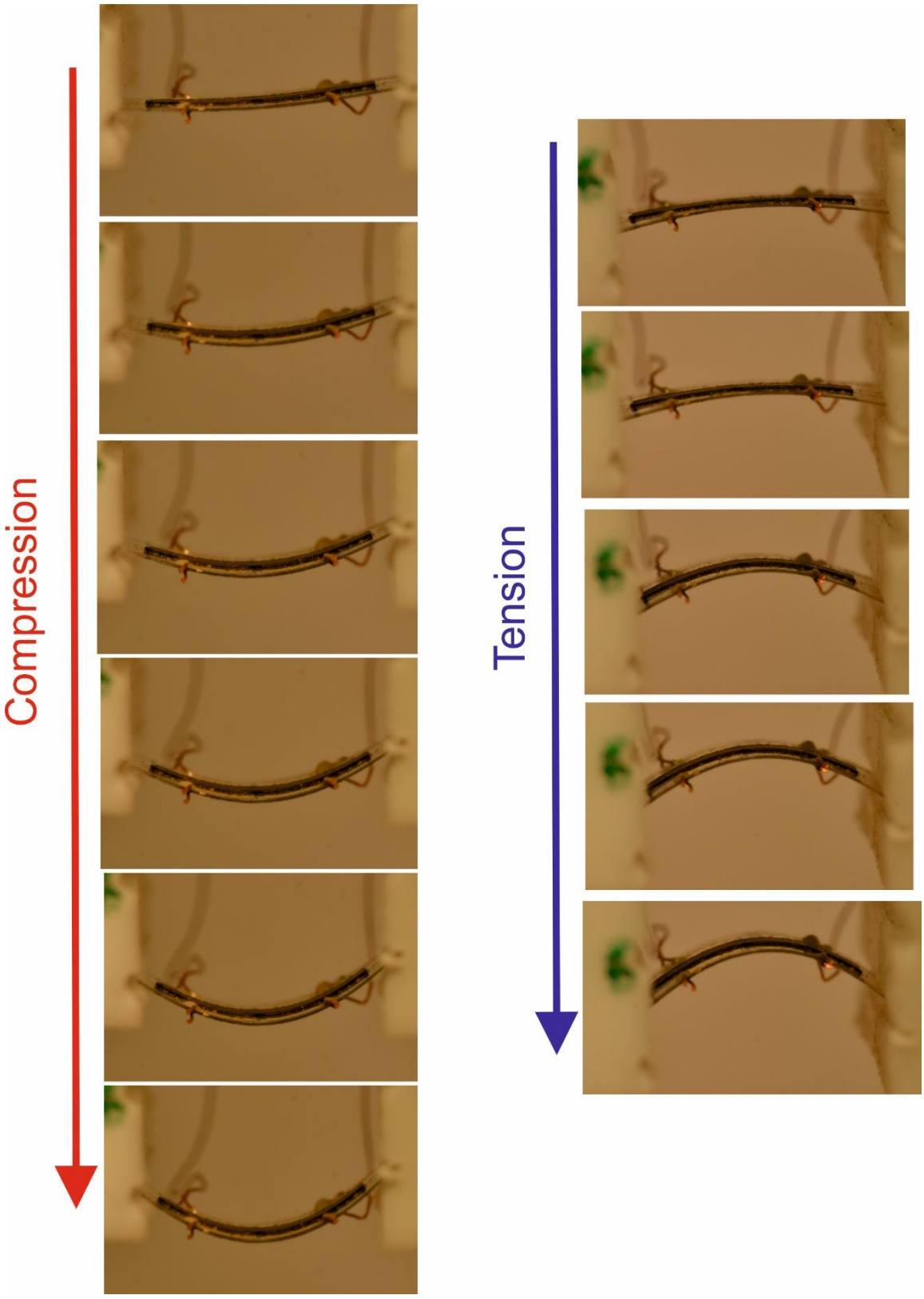

Figure S16 – **Piezoresistive film under compression and tension**